



# Sodium overload due to a persistent current that attenuates the arrhythmogenic potential of a novel LQT3 mutation

Adrien Moreau<sup>1</sup>, Andrew D. Krahn<sup>2</sup>, Pascal Gosselin-Badaroudine<sup>1</sup>, George J. Klein<sup>3</sup>, Georges Christé<sup>4</sup>, Yohann Vincent<sup>4</sup>, Mohamed Boutjdir<sup>5</sup> and Mohamed Chahine<sup>1\*</sup>

<sup>1</sup> Centre de Recherche de l'Institut Universitaire en Santé Mentale de Québec, Québec City, QC, Canada

<sup>2</sup> Division of Cardiology, University of British Columbia, Vancouver, BC, Canada

<sup>3</sup> Division of Cardiology, University of Western Ontario, London, ON, Canada

<sup>4</sup> Laboratoire de Neurocardiologie, Université Lyon, Lyon, France

<sup>5</sup> VA New York Harbor Healthcare System, SUNY Downstate Medical Center and NYU School of Medicine, New York City, NY, USA

## Edited by:

Hugues Abriel, University of Bern, Switzerland

## Reviewed by:

Arie O. Verkerk, Academisch

Medisch Centrum Universiteit van Amster, Netherlands

Said Bendahhou, Centre National de la Recherche Scientifique, France

Lars S. Maier,

Georg-August-Universität, Germany

## \*Correspondence:

Mohamed Chahine, Centre de Recherche de l'Institut Universitaire en Santé Mentale de Québec, 2601 Chemin de la Canardière, Québec City, QC G1J 2G3, Canada  
e-mail: mohamed.chahine@phc.ulaval.ca

Long QT syndrome (LQTS) is a congenital abnormality of cardiac repolarization that manifests as a prolonged QT interval on 12-lead electrocardiograms (ECGs). The syndrome may lead to syncope and sudden death from ventricular tachyarrhythmias known as *torsades de pointes*. An increased persistent Na<sup>+</sup> current is known to cause a Ca<sup>2+</sup> overload in case of ischemia for example. Such increased Na<sup>+</sup> persistent current is also usually associated to the LQT3 syndrome. The purpose of this study was to investigate the pathological consequences of a novel mutation in a family affected by LQTS. The impact of biophysical defects on cellular homeostasis are also investigated. Genomic DNA was extracted from blood samples, and a combination of PCR and DNA sequencing of several LQTS-linked genes was used to identify mutations. The mutation was reproduced *in vitro* and was characterized using the patch clamp technique and *in silico* quantitative analysis. A novel mutation (Q1476R) was identified on the *SCN5A* gene encoding the cardiac Na<sup>+</sup> channel. Cells expressing the Q1476R mutation exhibited biophysical alterations, including a shift of SS inactivation and a significant increase in the persistent Na<sup>+</sup> current. The *in silico* analysis confirmed the arrhythmogenic character of the Q1476R mutation. It further revealed that the increase in persistent Na<sup>+</sup> current causes a frequency-dependent Na<sup>+</sup> overload in cardiomyocytes co-expressing WT and mutant Na<sub>v</sub>1.5 channels that, in turn, exerts a moderating effect on the lengthening of the action potential (AP) duration caused by the mutation. The Q1476R mutation in *SCN5A* results in a three-fold increase in the window current and a persistent inward Na<sup>+</sup> current. These biophysical defects may expose the carrier of the mutation to arrhythmias that occur preferentially in the patient at rest or during tachycardia. However, the Na<sup>+</sup> overload counterbalances the gain-of-function of the mutation and is beneficial in that it prevents severe arrhythmias at intermediate heart rates.

**Keywords:** cardiac arrhythmia, electrophysiology, Na<sub>v</sub>1.5, long QT syndrome, LQT3, sodium overload, heart

## INTRODUCTION

In cardiomyocytes, action potentials (AP) ensure the propagation of excitation and the triggering of contraction. AP characteristics are directly related to the activity of voltage-gated sodium (Na<sup>+</sup>), calcium (Ca<sup>2+</sup>), and potassium (K<sup>+</sup>) channels (Amin et al., 2010). After a slight depolarization, voltage-gated Na<sup>+</sup> channels (Na<sub>v</sub>1.5), encoded by the *SCN5A* gene, activate, which leads to an inward Na<sup>+</sup> flow followed by a fast depolarization (Gellens et al., 1992). The AP is composed of a maintained depolarization, the “plateau” phase, followed by a final repolarization. The depolarization at the plateau is supported by a slowly decaying inward calcium current, background inward currents, and a persistent sodium current. The plateau is also supported by a delay in the onset of repolarizing potassium currents. The late activation of these potassium currents ensures final repolarization and causes

the membrane potential to return to the diastolic level after about 400 ms. The maintenance of action potential duration (APD) is critically related to the balance between depolarizing currents and repolarizing currents, so that an increase in depolarizing current(s) or a decrease in repolarizing current(s) will increase APD and, consequently, the QT interval of the electrocardiogram (ECG).

Long QT syndrome (LQTS) includes a congenital abnormality of cardiac repolarization that causes syncope and sudden death (Huang et al., 2011). This hereditary cardiac disease manifests as an increase in the QTc value over 450 ms on 12-lead ECGs, which points to an increase in the duration of ventricular APs. Under optimal conditions, QTc prolongation can induce ventricular tachyarrhythmia called *torsade de pointes* (TdP), which can degenerate into lethal ventricular fibrillation.

To date, mutations in thirteen genes have been identified as causing 13 types of LQTS (LQT1-13) (Schwartz et al., 2012) and are divided into three major groups: (1) mutations in genes encoding voltage-gated channels [*KCNQ1* (LQT1), *KCNH2* (LQT2), *SCN5A* (LQT3), *KCNJ2* (LQT7), *KCNJ5* (LQT13)], (2) mutations in genes encoding subunits regulating voltage-gated channel [*KCNE1* (LQT5), *KCNE2* (LQT6), *SCN4B* (LQT10)], and (3) mutations in genes encoding channel interacting proteins [*ANKB* (LQT4), *KCNE1* (LQT5), *KCNE2* (LQT6), *CAV3* (LQT9)].

*SCN5A* gene mutations can lead to several inherited cardiac diseases such as LQT3, Brugada syndrome (BrS) (Moreau et al., 2012), progressive cardiac conduction defect (CCD), sinus node disease, and dilated cardiomyopathy (DCM) (Amin et al., 2010; Gosselin-Badaroudine et al., 2012). In LQT3, a gain-of-function mediated by the appearance of a persistent current usually characterizes  $\text{Na}^+$  channel mutations. The persistent  $\text{Na}^+$  current has previously been shown to induce  $\text{Ca}^{2+}$  overload (Tang et al., 2012). Indeed, in hypoxia condition, the persistent  $\text{Na}^+$  current is increased and have been identified as a predominant cause of the deleterious  $\text{Ca}^{2+}$  overload (Tang et al., 2012). Such phenomenon could be important in the development of LQT3 syndrome and would be driven by the activation of  $\text{Na}^+/\text{H}^+$  and  $\text{Na}^+/\text{Ca}^{2+}$  exchangers. These exchangers are predominantly implicated in the  $\text{Ca}^{2+}$ ,  $\text{Na}^+$ , and pH regulation. However, most mutations in  $\text{K}^+$  channels or their regulatory subunits cause a loss-of-function characterized by a dominant negative effect. These biophysical defects lead to AP prolongation, creating a substrate for the development of ventricular arrhythmias (Schwartz et al., 2012).

The purpose of our study was to investigate the impact of a mutation causing LQTS in a patient and her family members using an *in vitro* heterologous expression system, the voltage-clamp technique, and *in silico* analysis. The biophysical investigation of the mutation in tsA201 cells revealed a positive shift in steady-state (SS) inactivation that results in an increased window current associated with the presence of a persistent  $\text{Na}^+$  current, which would explain the link between the mutation and LQTS in the family members. Furthermore, *in silico* experiments revealed that the persistent  $\text{Na}^+$  current induces an increase in the intracellular  $\text{Na}^+$  concentration. This causes an increase in repolarizing currents that shortens APD, counterbalancing the direct effect of the gain-of-function caused by the mutation and potentially benefitting the patient.

## METHODS

### CLINICAL EVALUATION

The proband and her family members underwent a detailed clinical and cardiovascular examination, including a 12-lead ECG, a determination of hemodynamic parameters, and laboratory blood tests. Echocardiography was used to exclude any structural heart disease. The QT interval was measured in lead II or V5 of the ECG and was corrected for the heart rate (QTc) using Bazett's formula. Exercise testing was performed to detect QT adaptation to heart rate changes, which is known to predict the genotype and direct therapy in LQTS (Schwartz et al., 2001; Wong et al., 2010).

The investigation conformed to the principles set out in the Declaration of Helsinki and was approved by the local institutional ethics committees on human subject research. The participants provided written informed consent prior to the study.

### GENOTYPING

The samples were sent to Genaissance Familion® (New Haven, CT, USA) for genetic testing of inherited cardiac syndromes. Genomic DNA was extracted and was amplified by PCR. Templates of the target exons, splice junctions, and flanking regions of *KCNQ1* (LQT1), *KCNH2* (LQT2), *SCN5A* (LQT3), *KCNE1* (LQT5), *KCNE2* (LQT6), *CACNA1C* (LQT8, exons 8 and 9), *CAV3* (LQT 9), *SCN4B* (LQT 10), *AKAP9* (LQT 11, exon 18), and *SNT12* (LQT 12) were generated and genotyped.

### MUTAGENESIS

Mutant  $\text{Na}_v1.5/\text{Q1476R}$  was generated using QuickChange TM site-directed mutagenesis kits according to the manufacturer's instructions (Stratagene, La Jolla, CA, USA). The  $\text{hNa}_v1.5/\text{mutants}$  were constructed from WT channels (NCBI accession number: M77235) using the following mutagenic sense and antisense primers (mutated sites are underlined):

1. 5'-CAACTTCAACCAACCGGAAGAAAAAGTTAGGG-3'
2. 5'-CCCTAACTTTTTTCTTCCGTTGGTTGAAGTTG-3'

Mutant and the wild-type (WT)  $\text{Na}_v1.5$  in a pcDNA3 construct were purified using Qiagen columns (Qiagen Inc., Chatsworth, CA, USA).

### TRANSFECTION OF THE tsA201 CELL LINE

TsA201 is a mammalian cell line derived from human embryonic kidney HEK 293 cells by stable transfection with SV40 large T antigen (Margolskee et al., 1993). The tsA201 cells were grown in high glucose DMEM supplemented with fetal bovine serum (10%), L-glutamine (2 mmol/L), penicillin (100 U/ml), and streptomycin (10 mg/ml) (Gibco BRL Life Technologies, Burlington, ON, Canada) and were incubated in a 5%  $\text{CO}_2$  humidified atmosphere. The cells were transfected using the calcium phosphate method (Margolskee et al., 1993), with the following modification to facilitate the identification of individual transfected cells: the cells were co-transfected with an expression plasmid for a lymphocyte surface antigen (CD8-a) (Jurman et al., 1994). The human  $\text{Na}^+$  channel  $\beta_1$  subunit and CD8 were constructed in the piRES vector (piRES/CD8/ $\beta_1$ ). With this strategy, transfected cells that bind beads also express the  $\beta_1$ -subunit. cDNA (5  $\mu\text{g}$ ) coding for the WT or mutant  $\text{Na}^+$  channel  $\alpha$ -subunit and 5  $\mu\text{g}$  of piRES/CD8/ $\beta_1$  were used. For the patch clamp experiments, 2 to 3-day-post-transfection cells were incubated for 5 min in a medium containing anti-CD8-a coated beads (Jurman et al., 1994) (Dynabeads M-450 CD8-a). Unattached beads were removed by washing. The beads were prepared according to the manufacturer's instructions (DynaL A.S., Oslo, Norway). Cells expressing surface CD8-a fixed the beads and were visually distinguishable from non-transfected cells by light microscopy.

## PATCH CLAMP TECHNIQUE

Macroscopic  $\text{Na}^+$  currents from tsA201-transfected cells were recorded using the whole-cell configuration of the patch clamp technique (Hamill et al., 1981). Patch electrodes were made from 8161 Corning borosilicate glass and were coated with HIPEC (Dow-Corning, Midland, MI, USA) to minimize their capacitance. Patch-clamp recordings were made using low resistance electrodes ( $<1\text{ M}\Omega$ ), and a routine series resistance compensation by an Axopatch 200 amplifier (Axon Instruments, Foster City, CA, USA) was performed to values  $>80\%$  to minimize voltage-clamp errors. Voltage-clamp command pulses were generated by microcomputer using pCLAMP software v10.0 (Axon Instruments).  $\text{Na}^+$  currents were filtered at 5 kHz, digitized at 10 kHz, and stored on a microcomputer equipped with an AD converter (Digidata 1300, Axon Instruments).

## SOLUTIONS AND REAGENTS

For whole cell recordings, the patch pipette contained (in mmol/L): 35 NaCl, 105 CsF, 10 EGTA, and 10 Cs-HEPES. The pH was adjusted to 7.4 using 1 N CsOH. The bath solution contained (in mmol/L) 150 NaCl, 2 KCl, 1.5  $\text{CaCl}_2$ , 1  $\text{MgCl}_2$ , 10 glucose, and 10 Na-HEPES. The pH was adjusted to 7.4 with 1 N NaOH. The recordings were made 5 min after establishing the whole cell configuration to allow the current to stabilize and to permit adequate diffusion of the contents of the patch electrode. All the recordings were made in the following order: I/V curve, SS inactivation, and recovery from inactivation. Experiments were carried out at room temperature (22–23°C).

## In silico analysis and AP modeling

The Priebe and Beuckelmann (1998) (PB), the Iyer et al. (2004) (IMW) model and the Ten Tusscher et al. (2004) (TNNP) models were considered as possible alternatives to represent human ventricular myocyte (Priebe and Beuckelmann, 1998; Iyer et al., 2004; Ten Tusscher et al., 2004). A comparison of these models was done by Ten Tusscher et al. in 2006 and it showed that the TNNP model was the most pertinent to reproduce the effects of IKr and IKs block on the human ventricular AP duration (Ten Tusscher et al., 2006). We considered it as a valid model to address changes related to LQT conditions. Besides, rather than using Markov models, this model is based on Hodgkin–Huxley equations, which are easy to adjust to known experimental data (Fink and Noble, 2009).

Thus, the *in silico* analysis was performed with the Ten Tusscher et al. (2004) model (Ten Tusscher et al., 2004), using the `tentusscher_noble_noble_panfilov_2004_a.cellml` file, ran in the COR environment (Peter Garny, <http://cor.physiol.ox.ac.uk/>).

Changes from the original set of equations are described in the Appendix.

When we attempted to modify the activation and inactivation parameters of the  $\text{Na}^+$  current (INa) in the original TNNP model, instabilities were found, which could not be resolved. Thus, the mathematical equations used for activation, inactivation, and recovery from inactivation of INa were taken from a stable guinea-pig ventricular cell model adjusted for 37°C (Pasek et al., 2008). However, the processes were accelerated two-fold (the time constants were reduced two-fold). This was done to

allow the model to reproduce the experimentally observed  $\text{Na}^+$  currents when we ran, in the model set for room temperature, the same voltage-clamp protocols as used in our *in vitro* experiments.

To adapt to the formalism of the  $\text{Na}^+$  current (INa) calculation that uses  $m^3$ , the measured values of the SS apparent activation variable measured in tsA201 cells were fitted with the following equation:  $m_{\text{inf}} = [1/(1 + \exp((V_m - V_h)/k))]^3$ , which yielded values of  $V_h = -59.1\text{ mV}$  and  $k = -7.9\text{ mV}$  for WT and  $V_h = -56.8\text{ mV}$  and  $k = -8.7\text{ mV}$  for Q1476R. This explains why these values of  $V_h$  and  $k$  were different from those calculated by fitting a simple Boltzmann function to data measured in tsA201 cells (Table 1).

Lastly, 5.5 mV was added to  $V_h$  and 0.5 mV to  $k$  to account for the difference in temperature given that the experiment was conducted at room temperature whereas the model was designed to work at 33°C, such that  $V_h = -59.1 + 5.5$  and  $k = -7.9 + 0.5$  for WT and  $V_h = -56.8 + 5.5$  and  $k = -8.7 + 0.5$  for Q1476R.

The SS inactivation functions were  $h_{\text{inf}} = 1/(1 + \exp((V_m - V_h)/k))$ , where  $V_h = -92.0 + 5.5$  and  $k = 4.4$  for WT, and  $V_h = -86.1 + 5.5$  and  $k = 4.3$  for Q1476R. In addition, 5.5 mV was added to  $V_h$  to account for the difference in temperature.

This adjustment of the kinetic parameters was derived from the detailed analysis of the effects of temperature on the activation and inactivation kinetics of  $\text{Na}_v1.5$  channels by Nagatomo et al. (1998). It reflects a change in temperature from 23 to 33°C. A linear extrapolation to 37°C could have been done. Nevertheless, no differences should be observed as these corrections would apply to both WT and mutated fast INa model equations.

The modeling of the heterozygous condition is based on the assumption that, in the carrier, both the WT and the mutated genes would lead to the presence of equal amounts of each corresponding channel protein. Thus, half of the fast  $\text{Na}^+$  current is characterized by the parameters of the WT channels while the second half is characterized by the parameters of the Q1476R channels.

The persistent part of the fast  $\text{Na}^+$  current was initially absent in the TNNP model. A persistent current was added that would not inactivate but that would activate and deactivate following

**Table 1 | Biophysical properties of  $\text{Na}_v1.5/\text{WT}$  and Q1476R.**

		WT (n = 13)	Q1476R (n = 14)
Peak current (pA/pF)		$-739.1 \pm 73.1$	$-690.8 \pm 69.9$
Persistent current (% I $\text{Na}^+$ )		$0.36 \pm 0.08$	$0.74 \pm 0.11^*$
Activation	$V_{1/2}$ (mV)	$-47.9 \pm 1.2$	$-46.3 \pm 1.1$
	$k$ (mV)	$-5.6 \pm 1.2$	$-6.5 \pm 0.4$
Inactivation	$V_{1/2}$ (mV)	$-92.0 \pm 1.3$	$-85.5 \pm 0.4^*$
	$k$ (mV)	$4.4 \pm 0.1$	$4.3 \pm 0.1$
Recovery from fast inactivation	A	$99.9 \pm 0.05$	$98.7 \pm 1.1$
	Tau	$2.7 \pm 0.1$	$2.2 \pm 0.3$

$V_{1/2}$ , Mid-point for activation or inactivation.

$k$ , Slope factor for activation or inactivation.

\*Difference between  $\text{Na}_v1.5/\text{WT}$  and  $\text{Na}_v1.5/\text{Q1476R}$  ( $p < 0.05$ ).

the same equations as the fast  $\text{Na}^+$  current (see equations in the Appendix).

Initially, the model was run with the basic set of values of variables and constants as used in the TNNP 2004a model, except for the formulation of  $\text{I}_{\text{Na}}$ , as described above. The  $\text{APD}_{90}$  was measured as the time between upstroke and 90% repolarization from the highest level of the plateau. No attempt was made to readjust the  $\text{APD}_{90}$  at SS at 1 Hz, which was increased from 322 ms in the original TNNP model to 454 ms for our WT settings.

Voltage-clamp testing was performed using MATLAB to show that the basic properties of the fast  $\text{I}_{\text{Na}}$  current, the persistent  $\text{Na}^+$  current and the window current, adjusted for room temperature, matched those of the WT and mutated currents as determined in the expression experiments when using the same protocols and measurement procedures in the presence of a realistic series resistance (not shown).

Based on our previous modeling experience with a persistent  $\text{I}_{\text{Na}}$  (Christe et al., 2008), it was necessary to allow the model to stabilize with a small amount of persistent  $\text{I}_{\text{Na}}$  before increasing the persistent  $\text{I}_{\text{Na}}$  until reaching at most one-third of the fraction of the fast peak  $\text{I}_{\text{Na}}$  observed in expression experiments. This was the maximal amount of persistent  $\text{I}_{\text{Na}}$  tolerated by the heterozygous mutation model in order to ensure that a stable AP was generated at 1 and 1.5 Hz.

## DATA ANALYSIS AND STATISTICS

The electrophysiological data were analyzed using macros in Clampfit (pCLAMP v10.0, Molecular Devices) and custom programs written using MATLAB (The MathWorks Inc.). Data are expressed as means  $\pm$  sem (standard error of the mean). Statistical comparison were performed using an unpaired Student's *t*-test or One-Way Anova with Bonferroni *post-hoc* test in Sigma plot (Jandel Scientific software). Differences were deemed significant at a *P*-value < 0.05.

## RESULTS

### CLINICAL CHARACTERISTICS OF THE INDEX PATIENT AND THE FAMILY MEMBERS

A 34-year-old female was assessed, in the context of a family history of sudden death, for a remote history of syncope after awakening to answer the telephone. Her sister had experienced a series of similar episodes at age 14 and had subsequently collapsed at rest and could not be resuscitated. The autopsy did not reveal a cause of death. A maternal cousin and grandaunt also experienced sudden death (Figure 1A). The resting QTc of the proband ranged from 450 to 485 ms and shortened to 422 ms at peak exercise. The echocardiogram was normal. Nadolol 40 mg once daily and mexiletine 200 mg twice daily were initiated. While mexiletine shortened the QTc (Figure 1B), it was discontinued before reassessment because of side effects. We identified an A-to-G base change at nucleotide position 5300 in exon 25 on the *SCN5A* gene by PCR and DNA sequencing. The base change led to a glutamine (Q)-to-arginine (R) substitution at residue 1476. The Q1476 residue is in a region of the *SCN5A* gene/ $\text{Na}_v1.5$  protein in  $\text{Na}^+$  channels (Figure 2A) that has been extraordinarily highly conserved throughout evolution, from humans to zebra fish (not shown). Another highly conserved glutamine (Q1475,

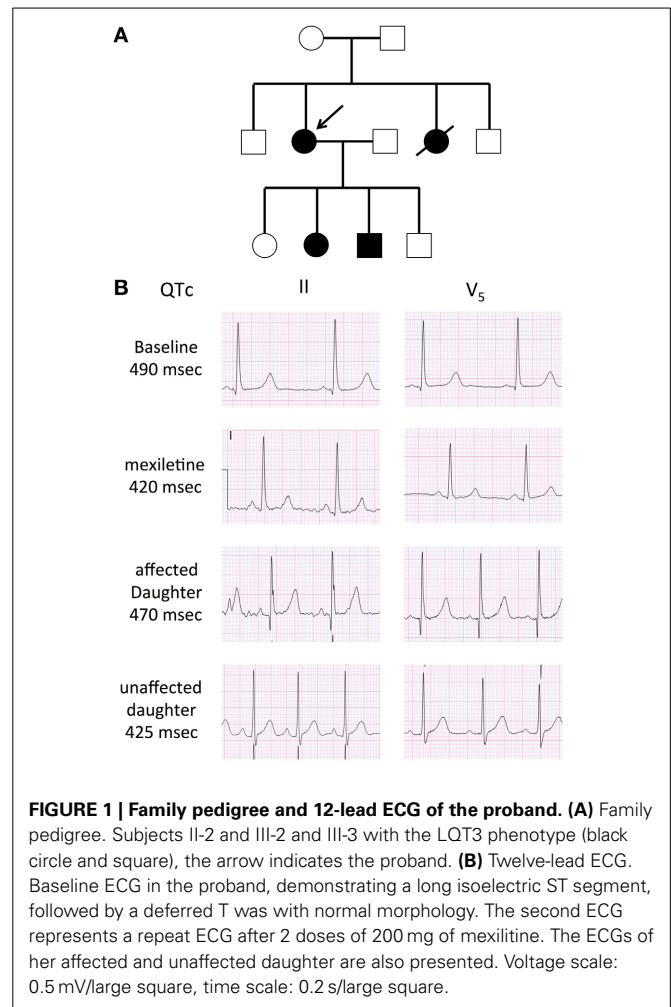


**FIGURE 1 | Family pedigree and 12-lead ECG of the proband. (A)** Family pedigree. Subjects II-2 and III-2 and III-3 with the LQT3 phenotype (black circle and square), the arrow indicates the proband. **(B)** Twelve-lead ECG. Baseline ECG in the proband, demonstrating a long isoelectric ST segment, followed by a deferred T wave with normal morphology. The second ECG represents a repeat ECG after 2 doses of 200 mg of mexiletine. The ECGs of her affected and unaffected daughter are also presented. Voltage scale: 0.5 mV/large square, time scale: 0.2 s/large square.

Figure 2A) was located upstream from the Q1476 residue. The mutation occurred in an important region of the  $\text{Na}^+$  channel known as the inactivation gate (Figure 2B). An H558R polymorphism was associated with the novel Q1476R mutation. The four children of the index patient were examined and presented QTc values of 414, 444, 480, and 502 ms. Three of them underwent an exercise test and their QTc values went from 444 to 442 ms, 480 to 500 ms, and 502 to 522 ms, respectively. The two who presented with borderline QTc prolongation were subsequently confirmed to be carrying the Q1476R variant. The index patient remained free of symptoms during the 5-year follow-up period.

### BIOPHYSICAL CHARACTERIZATION

We investigated whether the novel mutation caused an alteration of the biophysical properties of the  $\text{Na}_v1.5$   $\text{Na}^+$  channel that would explain the clinical phenotype of the index patient. Macroscopic  $\text{Na}^+$  currents were recorded from tsA201 cells expressing either WT ( $\text{Na}_v1.5/\text{WT}$ ) or mutant channels ( $\text{Na}_v1.5/\text{Q1476R}$ ) co-transfected with the regulatory  $\beta_1$ -subunit (see Methods for more details) (Figure 3A). The mutant  $\text{Na}^+$  channel current exhibited no significant shift in the current-voltage (*I/V*) relationship, and the current density was similar

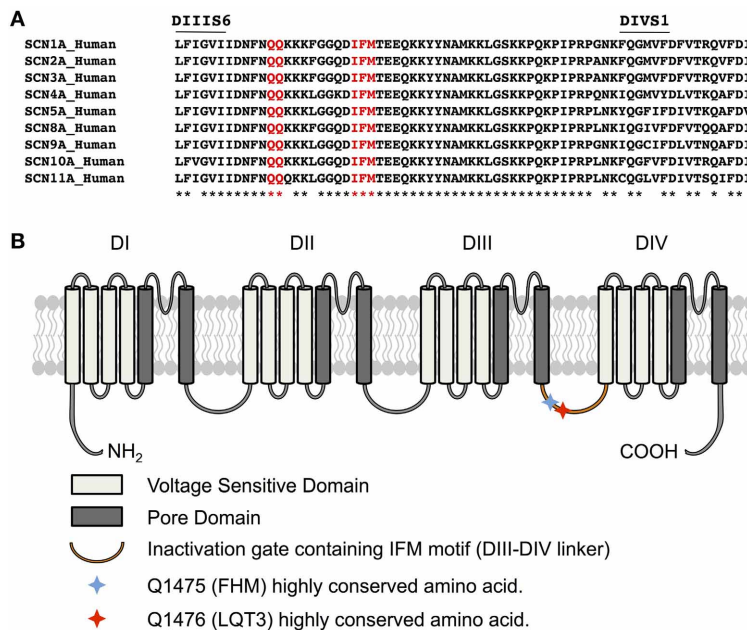


**FIGURE 2 | Q1476 is within a highly conserved region. (A)** Amino acid alignments of the region between transmembrane domains IIIS6 and IVS1 (III-IV linker) showing in red that glutamine 1475 and glutamine 1476 are highly conserved in human voltage-gated sodium channels. The IFM inactivation particle is displayed in red. **(B)** Schematic representation of the  $Na_v1.5$  channel structure displaying voltage

sensitive domains, the segments forming the pore domain, and the inactivation gate. Q1475 and Q1476 are also indicated. The missense mutation of one these two amino acids leads to several pathologies, depending on the channel impacted. The mutation of Q1475 in  $Na_v1.1$  causes familial hemiplegic migraine (FHM), whereas the mutation of Q1476 in  $Na_v1.5$  causes LQT3 syndrome.

to that of the WT channel (WT:  $-739.1 \pm 73.1$  pA/pF, Q1476R:  $-690.8 \pm 69.9$  pA/pF) (Figure 3B, Table 1). This result is based on the measurement of the peak current which is defined as the maximal absolute current obtained with the stimulation protocol (see Figure 3 legend). This peak current corresponds to the value where the global conductance reaches its maximum. A small persistent  $Na^+$  current was recorded. The persistent  $Na^+$  current was investigated using a 400 ms two-pulse protocol, and it was measured as mean of the current between 100 and 350 ms. The magnitude of this persistent current was significantly ( $p < 0.05$ ) different from that recorded from WT channels at  $-30$  mV ( $0.36 \pm 0.08\%$ ,  $n = 13$  for WT channels,  $0.74 \pm 0.11\%$ ,  $n = 14$  for mutant channels) (Figure 3C, Table 1). SS activation (Gv) and inactivation curves were also studied (Figure 3D, Table 1). The Gv curve of the mutant  $Na^+$  channel showed no significant shift ( $p = 0.340$  for  $V_{1/2}$  and  $p = 0.081$  for the slope factor). However, there was a 6.5 mV ( $p < 0.05$ ) shift in the SS inactivation curve toward more positive voltages for the Q1764R mutant channel ( $V_{1/2} Na_v1.5/Q1476R = -85.5 \pm 0.4$  mV,  $n = 14$  vs.  $V_{1/2} Na_v1.5/WT = -92.0 \pm 1.3$  mV,  $n = 13$ ). The slope factor was not significantly affected ( $p = 0.544$ ). The mutation did not induce any significant changes in the time course of the  $Na^+$  current decay or the recovery from inactivation (Figure 4).

The overlap of SS activation and inactivation of  $Na^+$  channels defines a range of voltages (i.e., window) where  $Na^+$  channels open, resulting in an inward  $Na^+$  current that could potentially depolarize the resting membrane potential and increase myocyte

excitability. The Q1476R mutation induced an increase in the overlap of  $Na^+$  channel activation and inactivation by shifting the inactivation to more positive potentials. This shift tended to expand the window and thus, the fraction of permanently activated channels. Figure 5A shows the predicted window currents of the WT and Q1476R mutant  $Na_v1.5$  channels. The Q1476R mutation produced a  $\sim 7$ -fold increase in the  $Na_v1.5$  window current, suggesting that more channels had reopened within the window region. Figure 5B shows the increase in the window current together with the increase in the persistent component, suggesting that Q1476R had a higher probability to open at voltages ranging from  $-140$  to  $+20$  mV.

The persistent  $Na^+$  current can be attributed to the  $Na_v1.5$  channel as it was blocked ( $0.06 \pm 0.06\%$ ,  $n = 5$ ) by  $10 \mu M$  of tetrodotoxin, a  $Na^+$  channel blocker (Figure 6). Mexiletine was seen to be efficient to treat the patient. The effect of this class I B antiarrhythmic was thus tested on the persistent  $Na^+$  current.  $50 \mu M$  of mexiletine importantly reduced the persistent  $Na^+$  current ( $0.09 \pm 0.03\%$ ,  $n = 5$ ) (Figure 6).

#### IN SILICO CHARACTERIZATION OF THE CHANGES INDUCED BY THE HETEROZYGOUS MUTATION Q1476R

The *in silico* characterization incorporates the heterozygous aspect of the mutation. This model is used to observe the effects of the mutation on several parameters including AP,  $Na^+$  window current  $I_{Na}$  (the large inward current surge simultaneous with AP upstroke is largely off scale), persistent  $Na^+$  current ( $I_{Nap}$ ),  $Na^+$  and  $Ca^{2+}$  intracellular concentrations ( $Na_i$  and  $Ca_i$ ). As a

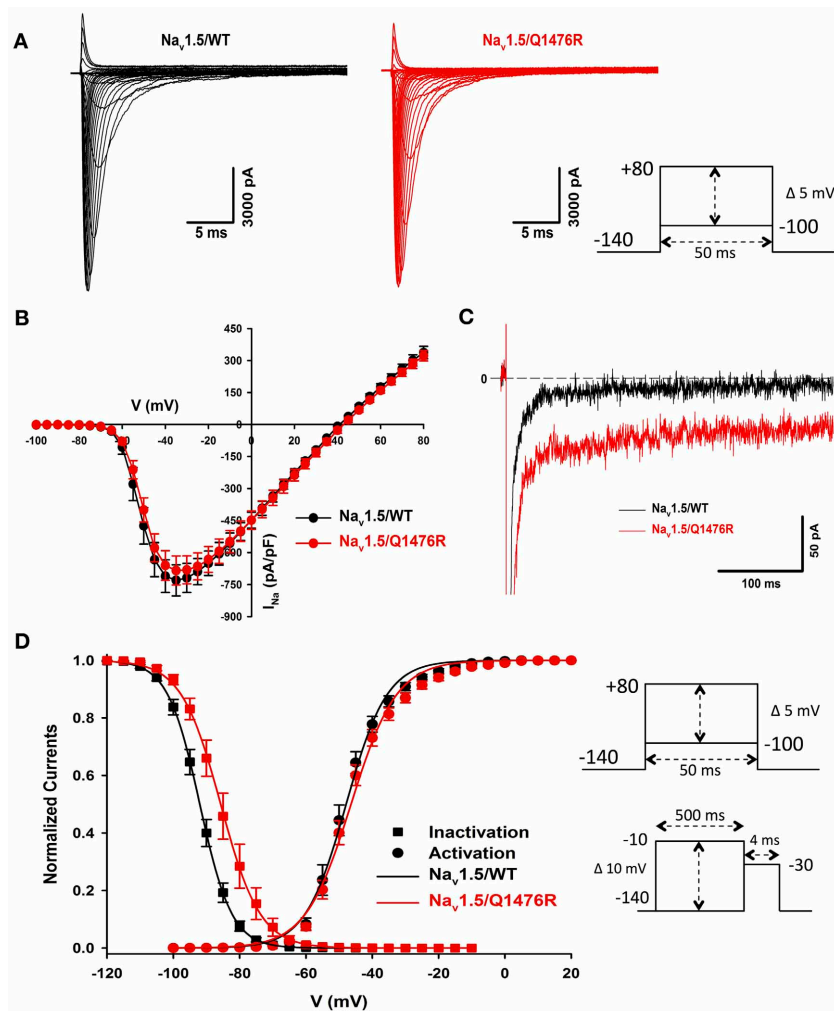


**FIGURE 3 | Biophysical characterization of Na<sub>v</sub>1.5/WT and the Q1476R mutant channels.** (A) Representative whole-cell current traces of the WT (left) and Q1476R (right) channels. Currents were elicited using a voltage-clamp protocol where depolarizing pulses were applied for 50 ms from -100 to +80 mV in 5 mV increments (see protocol in inset). The zero current corresponds to the basal line shown at the beginning of each trace. (B) After normalization to cell capacitance, current-voltage (I-V) relationships were constructed for the Na<sub>v</sub>1.5/WT ( $n = 13$ , black) and Q1476R ( $n = 14$ , red) channels. (C) Representative current traces obtained after a -30 mV depolarizing pulse showing I<sub>NaP</sub>. The Na<sub>v</sub>1.5/WT channel trace is depicted in black while the Na<sub>v</sub>1.5/Q1476R channel trace is depicted

in red. (D) Voltage dependence of SS activation (circles) or inactivation (squares) for the WT (black) and Q1476R (red) Na<sub>v</sub>1.5 Na<sub>v</sub>1.5 channels. A standard Boltzmann function was used to fit activation curves and to obtain the  $V_{1/2}$  and given in **Table 1** [ $G(V)/G_{max} = 1/(1 + \exp(-(V - V_{1/2})/k))$ ]. Inactivation currents were obtained by applying conditioning pre-pulses to membrane potentials ranging from a holding potential of -140 to -10 mV for 500 ms in 5 mV increments and were then measured using a 4-ms pulse to -30 mV at each step (see protocol in inset). The recorded inactivation values were fitted to a standard Boltzmann equation [ $I(V)/I_{max} = 1/(1 + \exp((V - V_{1/2})/k)) + C$ ] to obtain the values given in **Table 1**.

rule, model simulations were conducted for at least a 2000 s cell lifetime to ensure that SS in all variables was reached.

With 1-Hz stimulations, at SS, the WT model shows an APD<sub>90</sub> of 454 ms and a Na<sub>i</sub> of 11.94 mmol/L (central column, trace a, in **Figure 7A**, and **Table 2**). The model was then changed to the heterozygous condition (denoted as WR), with half of the I<sub>Na</sub> current being WT and half being Q1476R. The first AP obtained in the WR condition had an APD<sub>90</sub> of 587 ms (trace b) without appreciable change in Na<sub>i</sub>. Both Na<sup>+</sup> window current and I<sub>NaP</sub> amplitudes were increased when the mutation was introduced

(2nd and 3rd panels from the top, respectively, central column of **Figure 7A**). This was consistent with estimates computed from the voltage-clamp data (**Figure 5**). The difference is that the magnitude of the mutation-induced increase in the window current and in the I<sub>NaP</sub> as evaluated in the heterozygous model was two-fold less than that reported in **Table 1**, since, in the WR model, only half of the current is of the mutated type. When running this heterozygous model to SS (trace c), Na<sub>i</sub> expectedly increased, reaching 12.92 mmol/L, while APD<sub>90</sub> shortened to 513 ms. The diastolic Ca<sub>i</sub> and Ca<sub>i</sub> transients were also increased

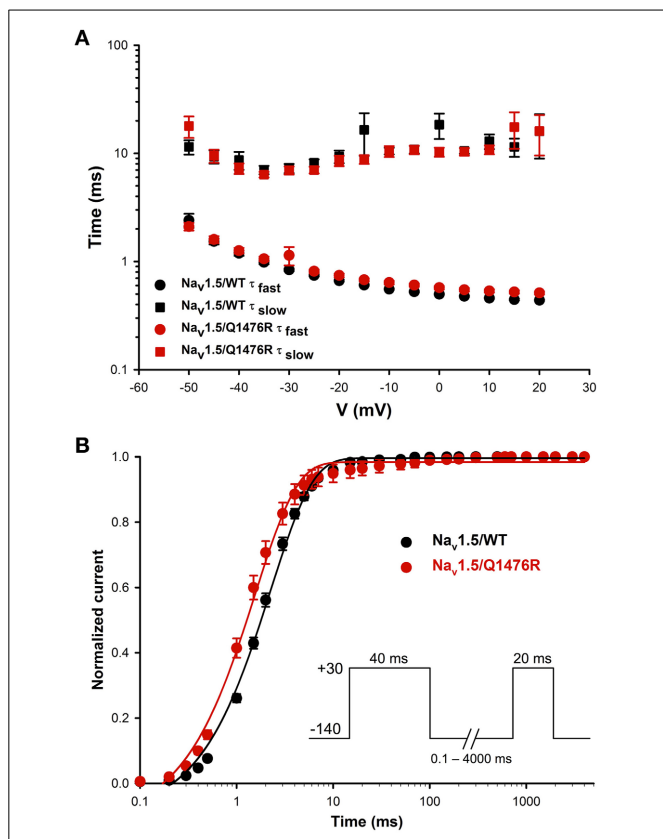
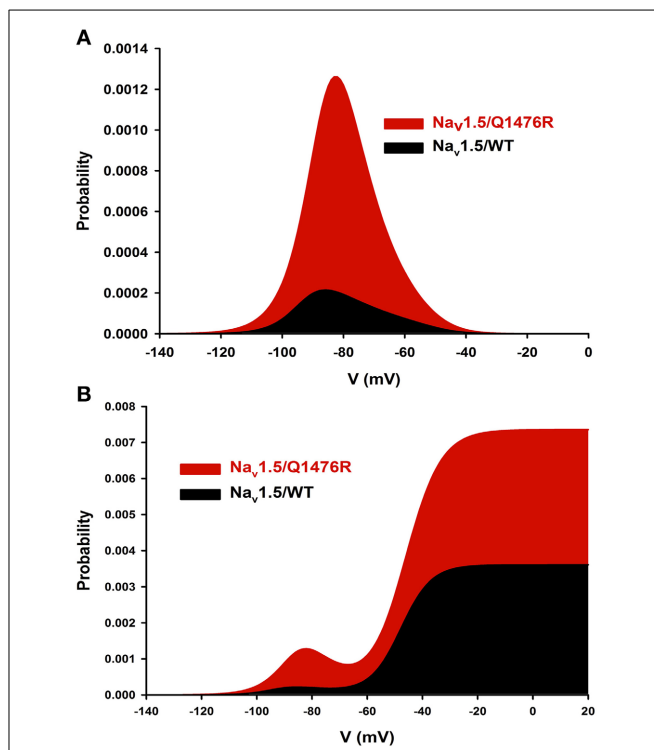


(**Figure 7A**, lower panel, central column and **Table 2**). The instantaneous  $APD_{90}$  lengthening by 29% due to changing from WT to WR condition was reduced to 13% *vs.* WT when the WR model reached SS. Most of the lengthening was thus counterbalanced by changes that occurred during regular stimulations for longer periods (typically 2000 s).

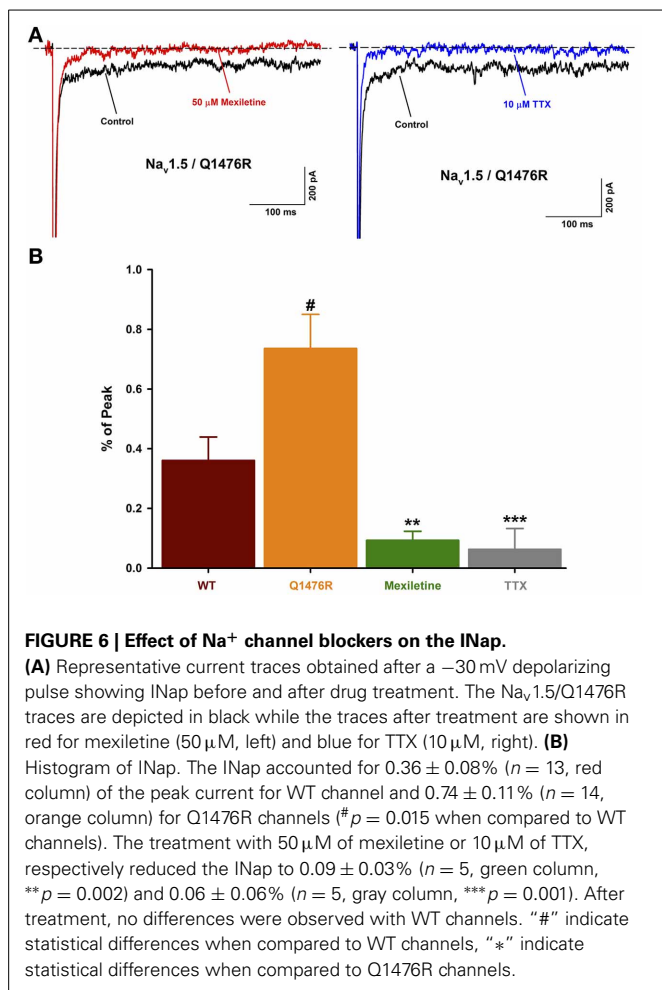
The same simulations were conducted at 1.5 Hz until SS (**Figure 7A**, 3rd column, and **Table 2**).  $APD_{90}$  and  $Na_i$ , respectively stabilized at 392 ms and 13.59 mmol/L for WT (trace a). After the switch to the WR model, the first AP (trace b) had an  $APD_{90}$  of 471 ms ( $Na_i$  remained unchanged). After reaching SS (trace c),  $APD_{90}$  shortened to 436 ms and  $Na_i$  increased to 14.57 mmol/L. At SS, the diastolic  $Ca_i$  and  $Ca_i$  transients had increased in the WR model. The increases were larger than



those seen at 1 Hz (**Figure 7A**, lower panel, 3rd column and **Table 2**).

To test the effect of bradycardia, the stimulation rate was lowered from 1 Hz to 0.5 Hz. At SS, the WT model had a longer  $APD_{90}$  (558 ms) and a lower  $Na_i$  (9.84 mmol/L) than at 1 Hz. In the WR model at 0.5 Hz,  $APD_{90}$  and  $Na_i$  reached SS values of 705 ms and 10.95 mmol/L (**Table 3**), while the diastolic  $Ca_i$  and  $Ca_i$  transients decreased (**Figure 7A**, 1st column, lower panel and **Table 3**). To determine the effect of changes in  $Na_i$  on  $APD_{90}$ , changes in  $Na_i$  were applied instantaneously to the model in several settings (**Figure 7B**).

In the WT model, from SS at 1 Hz, setting  $Na_i$  to its value at SS at 0.5 Hz produced an  $APD_{90}$  of 542 ms (**Figure 7B**, left panel). This was comparable to the SS  $APD_{90}$  at 0.5 Hz when  $Na_i$  was not imposed (558 ms). Likewise, when SS  $Na_i$  was imposed in the WR model at 0.5 and 1 Hz, the  $APD_{90}$ s of the next AP were respectively 683 and 515 ms, *vs.* 705 and 513 ms at SS when  $Na_i$  was not imposed (left panel of **Figure 7B** and **Table 3**). At 1 Hz, in WR model under SS, changing  $Na_i$  to WT SS value produced  $APD_{90}$  of 582 ms. This value is close to that of the first WR AP ( $APD_{90}$  of 587 ms). Then, changing to WT produced  $APD_{90}$  of 451 ms which is similar to SS WT  $APD_{90}$  of 454 ms (middle panel of **Figure 7B** and **Table 1**). At 1.5 Hz (**Figure 7B**, right panel and **Table 2**),  $APD_{90}$  produced by changing  $Na_i$  values were very close



to those in the original simulations at SS. Thus, applying solely Na<sub>i</sub> changes reproduced most of the APD<sub>90</sub> decrease observed at SS.

In the TNNP 2004 model, the only two ion transfer mechanisms that depend on Na<sub>i</sub> are the Na<sup>+</sup>-K<sup>+</sup> pump (INaK) and the Na<sup>+</sup>-Ca<sup>2+</sup> exchanger (INaCa) (Ten Tusscher et al., 2004). Their activity increase when Na<sub>i</sub> is increased. In **Figure 8A**, the two upper panels are a repeat of the first and third panels from the top in the middle column of **Figure 7**. The lower panel of **Figure 8A** is new and reports the time course of the INaK and INaCa currents during an AP. There was a large immediate increase in the duration of the first AP recorded after switching the model to the WR condition (**Figure 8A** upper panel, compare traces a and b). This was a direct effect of the increase in the conductance of the INap (middle panel, blue vs. black trace). The magnitudes of the INaK and the INaCa exchanger currents followed the changes in the membrane potential (compare blue and black traces in the lower panel). We further stimulated the model at 1 Hz until SS. The APD<sub>90</sub> shortened (**Figure 8A** upper panel, trace c, orange line). While the changes in INap magnitude just followed the changes in membrane voltage values (orange vs. blue trace, middle panel), the magnitudes of both the INaK and the INaCa currents increased (orange vs. blue trace, lower panel).

The increase in the INaK current was small compared to the 30% increase in the magnitude of the INaCa exchanger current.

As seen in **Figure 7**, there was a concomitant raise in the diastolic Ca<sub>i</sub> and in the Ca<sub>i</sub> transients in tandem with the increase in Na<sub>i</sub> when the stimulations were applied until SS. To isolate the effect of the increase in Na<sub>i</sub>, we started with the WR model stabilized at 1 Hz and instantaneously changed Na<sub>i</sub> to that of the SS WT model (**Figure 8B**, black to blue traces). The model was then instantaneously returned to the WT model (**Figure 8B**, blue to orange traces). The changes in APD<sub>90</sub>, INaK, and INaCa were comparable to those in **Figure 8A**. This indicates that, when Na<sub>i</sub> was increased, the reverse mode of INaCa provided the main increase in the outward current that caused the shortening of the APD<sub>90</sub>.

A possible contribution of the increase in window current in the effects of the mutation was tested in the model at steady-state at 1 Hz. The diastolic membrane voltage in the WT situation was  $-85.9$  mV and the threshold for stimulation was 21.4 pA/pF, whereas in the WR situation, they were  $-85.5$  mV and 20.8 pA/pF, respectively. Thus, there was a 0.4 mV depolarization and a 2.8% decrease in stimulation threshold. Further, when the window current of the WR model was made identical to that in the WT model, by suppressing any changes in steady-state activation and inactivation curves, the diastolic membrane voltage was  $-85.7$  mV and stimulation threshold 21.3 pA/pF. Thus, although slightly, the window current appeared to increase cell excitability.

## DISCUSSION

We biophysically characterized a novel LQT3 mutation (Q1476R) found in a previously symptomatic 34-year-old female with a classic LQT3 ECG phenotype. The Q1476 residue is a highly conserved amino acid in all Na<sup>+</sup> channels (**Figure 2**) throughout evolution, from humans to zebra fish. Interestingly, a second highly conserved Q residue (Q1475) (**Figure 2**) was found immediately upstream from Q1476. These two residues were located in the inactivation gate upstream from the IFM motif. Given their location, they are likely to play a role in the inactivation process. Moreover, the Q1489H missense substitution on SCN1A encoding the Na<sub>v</sub>1.1 neuronal voltage-gated Na<sup>+</sup> channel (the Q1475 homolog in Na<sub>v</sub>1.5) is highly expressed in the central nervous system, including the retina, and is found in patients with familial hemiplegic migraine (FHM, **Figure 2B**) (Vahedi et al., 2009). Unfortunately, no biophysical characterization has been reported for this mutation. We can speculate that a gain-of-function due to this mutation may be the cause of FHM.

The present paper provides support for the concept that the increase in the window current and the increase in the TTX sensitive persistent current due to the LQT3 mutation (Q1476R) cause LQTS. This is consistent with all studies indicating that mutations in SCN5A causing LQTS are related to a gain-of-function (Schwartz et al., 2012).

The treatment with 50  $\mu$ M of mexiletine importantly reduced the INap observed on Q1476R mutant channels. This might explain the beneficial effects of mexiletine treatment on the patient. Unfortunately, the nausea due to mexiletine have imposed the discontinuation of the treatment.

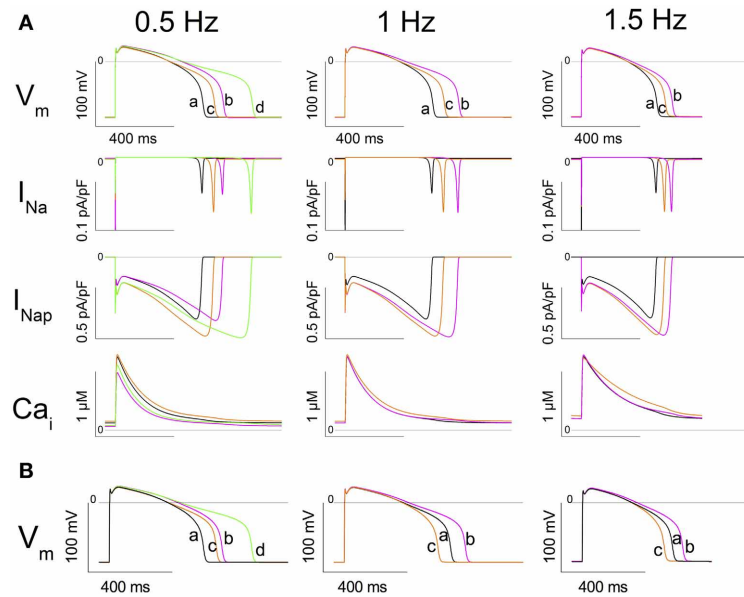


**FIGURE 7 | In silico simulation of heterozygous cardiomyocytes carrying the Q1476R mutation. (A)** The three columns correspond to different stimulation frequencies indicated at the top of the figure. From top to bottom: the action potential (AP), the fast sodium current (INa), the persistent sodium current (INap), and cytosolic [Ca<sup>2+</sup>] (Ca<sub>i</sub>). Under column 0.5 Hz, traces at SS are superimposed: trace a: WT at 1 Hz (black), trace b: WT at 0.5 Hz (magenta), trace c: WR (1/2 WT + 1/2 Q1476R) at 1 Hz (orange), and trace d: WR at 0.5 Hz (green). Under column 1 Hz, trace a is WT at SS at 1 Hz, trace b is the subsequent AP after changing the model to WR, and trace c is the SS in WR at 1 Hz. Under column 1.5 Hz, trace a is WT at SS at 1.5 Hz, trace b is the subsequent AP after changing the model to WR, and trace c is the SS in WR at 1.5 Hz. **(B)** Model tests of the role of Na<sub>i</sub> in determining APD<sub>90</sub>. Instead of running the model until SS, Na<sub>i</sub> is changed instantaneously to its SS value. *Left panel*, trace a shows the SS AP in WT at 1 Hz. Trace b shows

the subsequent AP recorded after changing Na<sub>i</sub> to the value previously observed at SS in the WT model at 0.5 Hz (9.84 mmol/L). Trace c shows the subsequent AP recorded from the model after simultaneously setting the model to WR and changing Na<sub>i</sub> to the value for WR at 1 Hz at SS (12.92 mmol/L). Trace d shows the next AP recorded after changing Na<sub>i</sub> to the value previously observed at SS in WR at 0.5 Hz (10.95 mmol/L). *Middle panel*, trace a shows the SS AP in WR at 1 Hz. Trace b shows the subsequent AP recorded after changing Na<sub>i</sub> to its value previously observed at SS in the WT model at 1 Hz (11.94 mmol/L). Trace c is the subsequent AP recorded from the model after setting the model to WT. *Right panel*: Trace a shows the SS AP in WR at 1.5 Hz. Trace b shows the subsequent AP recorded after changing Na<sub>i</sub> to the value previously observed at SS in the WT model at 1.5 Hz (13.59 mmol/L). Trace c shows the subsequent AP recorded from the model after setting the model to WT.

**Table 2 | APD<sub>90</sub>, Na<sub>i</sub>, and diastolic Ca<sub>i</sub> at steady state recorded in the model during 1- and 1.5-Hz stimulation.**

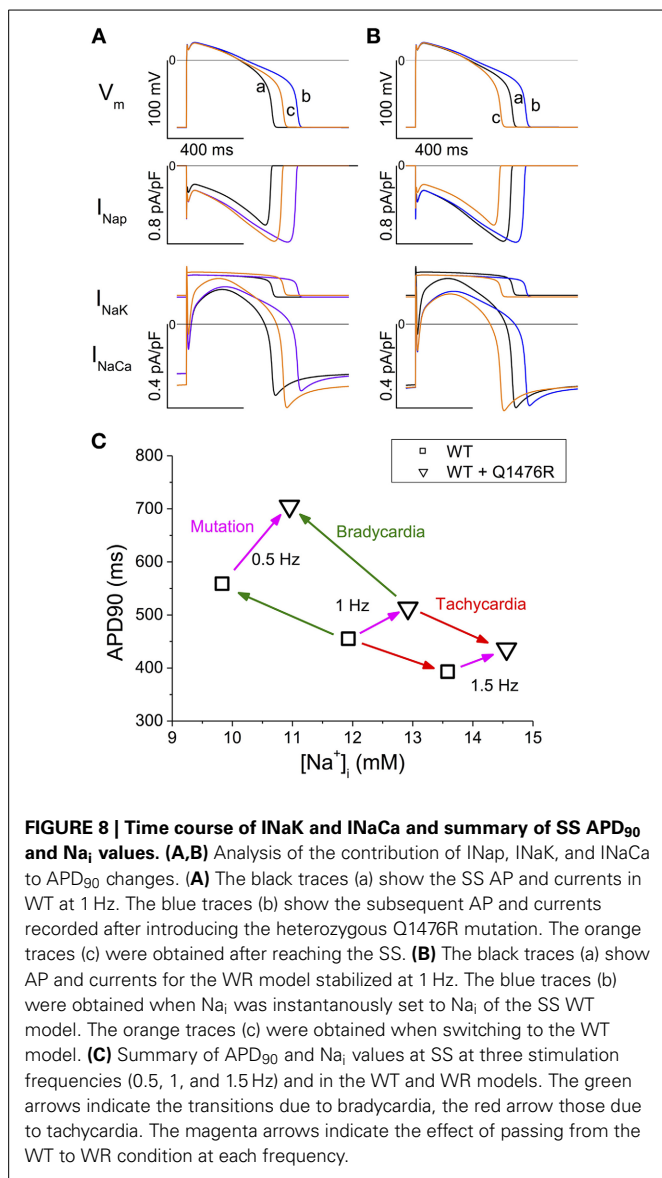
Stimulation frequency	Parameter	WT	WR first AP	WR
1 Hz	APD <sub>90</sub> (ms)	454	587	513
	Na <sub>i</sub> (mmol/L)	11.94	11.94	12.92
	Diastolic Ca <sub>i</sub> (μmol/L)	0.109	0.109	0.135
	APD <sub>90</sub> in Na <sub>i</sub> tests (ms)	451	582	
1.5 Hz	APD <sub>90</sub> (ms)	392	471	436
	Na <sub>i</sub> (mmol/L)	13.59	13.59	14.57
	Diastolic Ca <sub>i</sub> (μmol/L)	0.179	0.177	0.221
	APD <sub>90</sub> in Na <sub>i</sub> tests (ms)	396	484	

**Table 3 | Effect of bradycardia on APD<sub>90</sub>, Na<sub>i</sub>, and diastolic Ca<sub>i</sub> at steady state.**

	WT at 1 Hz	WT at 0.5 Hz	WR at 1 Hz	WR at 0.5 Hz
APD <sub>90</sub> (ms)	454	558	513	705
Na <sub>i</sub> (mmol/L)	11.94	9.84	12.92	10.95
Diastolic Ca <sub>i</sub> (μmol/L)	0.109	0.057	0.135	0.071
APD <sub>90</sub> in Na <sub>i</sub> test (ms)		542	515	683

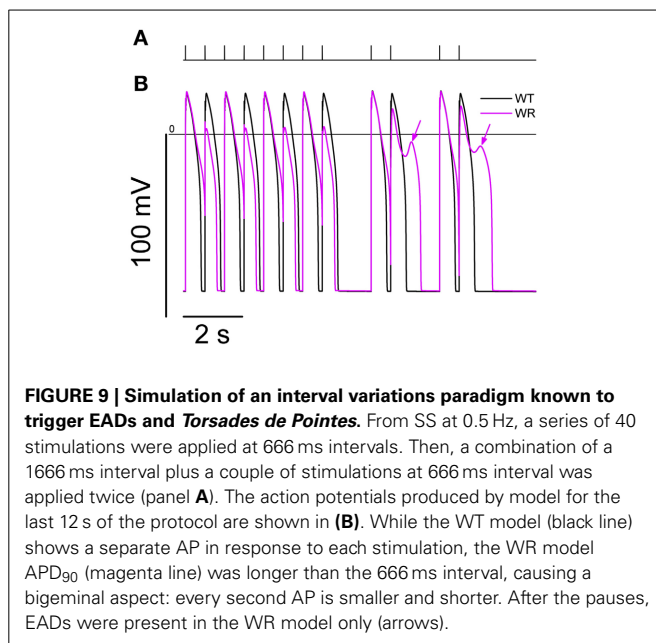
As expected from its localization, the mutation impacts the inactivation process. The Q1476R mutation resulted in a depolarizing shift of inactivation, which tended to increase the overlap of activation and inactivation gating (Figure 5). At voltages within this overlap region, Na<sup>+</sup> channels are partially but not fully inactivated, thus increasing the potential for persistent window

currents (Attwell et al., 1979). At -50 mV, the peak window current probability predicts that a small percentage (0.1%) of the mutant channels will be persistently activated. The resulting inward Na<sup>+</sup> current at resting membrane potentials could depolarize cardiac myocytes, leading to an increase in their excitability. The increase in persistent current is not surprising as the mutation is localized in the inactivation gate (DIII-DIV linker). The effect of this mutation on the inactivation process would be a decrease of the probability for channels to enter an inactivated state. Consequently, a small amount of Na<sub>v</sub>1.5 Q1476R channels will not inactivate after the rapid activation. Similar mechanisms



are believed to underlie the increased excitability of sensory neurons harboring inherited human pain disorder mutations that produce shifts in Na<sub>v</sub>1.7 activation and inactivation of similar polarity and magnitude as those observed in the present study (Harty et al., 2006; Rush et al., 2006; Dib-Hajj et al., 2010).

The *in silico* model confirmed the arrhythmogenic potential of the Q1476R mutation. When the model was changed to the heterozygous mutated paradigm, there was an immediate effect that prolonged APD<sub>90</sub>. Continued stimulation caused a partial reversion of this effect when SS was reached. At the same time, both Na<sub>i</sub> and Ca<sub>i</sub> increased. **Figure 8C** summarizes the effects of the mutation combined with the heart rate on APD<sub>90</sub> and Na<sub>i</sub>. At SS, the accumulation of Na<sup>+</sup> ions, related both to an elevated frequency and to the presence of the mutation, tended to shorten APD<sub>90</sub>. This would in turn tend to moderate the LQT effect of the mutation at elevated heart rates such as under effort or moderate stress. The gain-of-function due to a persistent



Na<sup>+</sup> current may thus protect against arrhythmogenesis related to a limited increase in heart rate. However, as was seen in the model, an overload of Ca<sub>i</sub> stores may appear at higher rates and may trigger arrhythmias (Christe et al., 2008). Our data are consistent with published experimental and model studies (Pieske and Houser, 2003; Noble and Noble, 2006; Undrovinas et al., 2006; Soliman et al., 2012). When combined with elevated Ca<sup>2+</sup> entry under adrenergic stress, arrhythmias may appear due to early or late after-depolarizations. Under elevated Ca<sub>i</sub> conditions, a decrease in the L-type Ca<sup>2+</sup> current ought to take place due to the decrease in the transmembrane [Ca<sup>2+</sup>]<sub>i</sub> gradient and to the accelerated decay by calcium-dependent inactivation. Nevertheless, its contribution to the overall effect should be minor. The slowly activating potassium current I<sub>Ks</sub> was shown to be increased by elevation of Ca<sub>i</sub>, as due to a relief of KCNQ1 inactivation by calmodulin in a Ca<sup>2+</sup> dependent way (Ghosh et al., 2006). This feature was absent in the model. Such an effect would enhance the frequency-dependent effect observed in the model, resulting into a further shortening of the AP at high frequencies that would be larger in the WR than in the WT situation.

A combination of interval variations known to trigger EADs and *torsades de pointes* (El-Sherif et al., 1999; Viswanathan and Rudy, 1999; Tan et al., 2006) has been tested in the model. EADs appeared in the WR condition while the WT remained unaffected (**Figure 9**). This is consistent with emotional stress and exercise as known triggers of arrhythmias in LQT3 (Schwartz et al., 2001).

Conversely, bradycardia causes a lower Na<sub>i</sub> and a lengthening of APD, which are well-known features of bradycardia (Faber and Rudy, 2000). Changes in diastolic Ca<sub>i</sub> and Ca<sub>i</sub> transients are also observed. Each of these may change the magnitude of ionic currents and exchangers. Elevated Na<sub>i</sub> is known to cause an activation of the Na/K ATPase pump and an increase in the reverse mode Na-Ca exchanger current. Both of these processes

may shorten APD (Armoundas et al., 2003), as well as the increase in  $\text{Ca}^{2+}$ -dependent inactivation of the  $\text{Ca}^{2+}$  current due to elevated  $\text{Ca}_i$  (Carmeliet, 2006). Our simulations showed that most of the APD changes were due to changes in  $\text{Na}_i$ , mainly through a lower  $\text{INaCa}$ . The LQT effect of the mutation is likely to be more serious at low heart rates, as illustrated in our simulations where  $\text{APD}_{90}$  reached very critical values around 700 ms in the heterozygous model. Thus, the carrier of the mutation may be preferentially sensitive to factors triggering arrhythmias when at rest, which is a characteristic of LQT3 syndrome. During activity, APD shortening, due to increased entry of  $\text{Na}^+$  ions, may protect the carrier against arrhythmias. These results should be qualitatively reproduced in other models of human ventricular myocytes, since the basic features of the  $\text{Na}_i$  homeostasis ought to obey to the same constraints. Furthermore, the functional consequences, as analyzed here for mutation Q1476R, may in principle be extended for other LQT3 mutations involving an increase in persistent and window currents. The intracellular  $\text{Na}^+$  overload, as related to the gain-of-function in  $\text{Na}^+$  channels, is proper to LQT3 and is unlikely in LQT syndromes related to potassium channel dysfunctions. This might be taken into account for personalized prevention and therapy of LQT3 patients.

#### LIMITATIONS OF THE *IN SILICO* MODEL

The basic TNNP model assumed no fraction of  $\text{INaP}$ . However, the magnitudes of the  $\text{INaCa}$ ,  $\text{INaK}$ , and  $\text{Na}^+$  background currents had been adjusted to account for the high  $\text{Na}_i$  in ventricular human myocytes. The present modified model may thus have an

overall excess of  $\text{Na}^+$  entry. A late  $\text{Na}^+$  current was added to the model in the WT condition, and its magnitude was limited to one-third of the fraction of the peak  $\text{Na}^+$  current found in tsA201 cells. This caused the  $\text{APD}_{90}$  in the WT configuration to be 454 ms vs. 325 ms in the basic TNNP model, whereas values of  $\sim 370$  or 400 ms have been reported by Li et al. (1998, 1999) in human ventricular myocytes. As a result, the effects of the mutation may have been overemphasized in the present simulations.

Several ion channels have been shown to be modulated by intracellular  $\text{Ca}^{2+}$ , either directly or through intracellular effectors (e.g., calmodulin), such modulations were not included in the model. Several additional channels (e.g., stretch-sensitive channels) found in mammalian ventricular myocytes were neither included. A number of investigations in human ventricular myocytes are still needed to document their formulation.

Lastly, this model assumes that no changes other than those due to the  $\text{Na}^+$  channel mutation took place. There are reasons to doubt this, since a permanent  $\text{Na}^+$  and  $\text{Ca}^{2+}$  overload, as seen here in the WR model, are known triggers of remodeling of ion channel densities and excitation-contraction coupling efficiency in cardiac cells, which may have taken place over the long-term in carriers of the mutation.

#### ACKNOWLEDGMENTS

This study was supported by grants from the Heart and Stroke Foundation of Quebec (HSFQ), the Canadian Institutes of Health Research (CIHR, MT-13181), and the Heart and Stroke Foundation of Ontario (T6730).

#### REFERENCES

- Amin, A. S., Asghari-Roodsari, A., and Tan, H. L. (2010). Cardiac sodium channelopathies. *Pflugers Arch.* 460, 223–237. doi: 10.1007/s00424-009-0761-0
- Armoundas, A. A., Hobai, I. A., Tomaselli, G. F., Winslow, R. L., and O'Rourke, B. (2003). Role of sodium-calcium exchanger in modulating the action potential of ventricular myocytes from normal and failing hearts. *Circ. Res.* 93, 46–53. doi: 10.1161/01.RES.0000080932.98903.D8
- Attwell, D., Cohen, I., Eisner, D., Ohba, M., and Ojeda, C. (1979). The steady state TTX-sensitive ("window") sodium current in cardiac Purkinje fibres. *Pflugers Arch.* 379, 137–142. doi: 10.1007/BF00586939
- Carmeliet, E. (2006). Action potential duration, rate of stimulation, and intracellular sodium. *J. Cardiovasc. Electrophysiol.* 17(Suppl. 1), S2–S7. doi: 10.1111/j.1540-8167.2006.00378.x
- Christe, G., Chahine, M., Chevalier, P., and Pasek, M. (2008). Changes in action potentials and intracellular ionic homeostasis in a ventricular cell model related to a persistent sodium current in SCN5A mutations underlying LQT3. *Prog. Biophys. Mol. Biol.* 96, 281–293. doi: 10.1016/j.pbiomolbio.2007.07.023
- Dib-Hajj, S. D., Cummins, T. R., Black, J. A., and Waxman, S. G. (2010). Sodium channels in normal and pathological pain. *Annu. Rev. Neurosci.* 33, 325–347. doi: 10.1146/annurev-neuro-060909-153234
- El-Sherif, N., Caref, E. B., Chinushi, M., and Restivo, M. (1999). Mechanism of arrhythmogenicity of the short-long cardiac sequence that precedes ventricular tachyarrhythmias in the long QT syndrome. *J. Am. Coll. Cardiol.* 33, 1415–1423. doi: 10.1016/S0735-1097(98)00700-1
- Faber, G. M., and Rudy, Y. (2000). Action potential and contractility changes in  $[\text{Na}^+]_i$  overloaded cardiac myocytes: a simulation study. *Biophys. J.* 78, 2392–2404. doi: 10.1016/S0006-3495(00)76783-X
- Fink, M., and Noble, D. (2009). Markov models for ion channels: versatility versus identifiability and speed. *Philos. Trans. A Math. Phys. Eng. Sci.* 367, 2161–2179. doi: 10.1098/rsta.2008.0301
- Gellens, M. E., George, A. L. Jr., Chen, L. Q., Chahine, M., Horn, R., Barchi, R. L., et al. (1992). Primary structure and functional expression of the human cardiac tetrodotoxin-insensitive voltage-dependent sodium channel. *Proc. Natl. Acad. Sci. U.S.A.* 89, 554–558. doi: 10.1073/pnas.89.2.554
- Ghosh, S., Nunziato, D. A., and Pitt, G. S. (2006). KCNQ1 assembly and function is blocked by long-QT syndrome mutations that disrupt interaction with calmodulin. *Circ. Res.* 98, 1048–1054. doi: 10.1161/01.RES.0000218863.44140.f2
- Gosselin-Badaroudine, P., Keller, D. I., Huang, H., Pouliot, V., Chatelier, A., Osswald, S., et al. (2012). A proton leak current through the cardiac sodium channel is linked to mixed arrhythmia and the dilated cardiomyopathy phenotype. *PLoS ONE* 7:e38331. doi: 10.1371/journal.pone.0038331
- Hamill, O. P., Marty, A., Neher, E., Sakmann, B., and Sigworth, F. J. (1981). Improved patch-clamp techniques for high-resolution current recording from cells and cell-free membrane patches. *Pflugers Arch.* 391, 85–100. doi: 10.1007/BF00656997
- Harty, T. P., Dib-Hajj, S. D., Tyrrell, L., Blackman, R., Hisama, F. M., Rose, J. B., et al. (2006).  $\text{Na}(V)1.7$  mutant A863P in erythromelalgia: effects of altered activation and steady-state inactivation on excitability of nociceptive dorsal root ganglion neurons. *J. Neurosci.* 26, 12566–12575. doi: 10.1523/JNEUROSCI.3424-06.2006
- Huang, H., Priori, S. G., Napolitano, C., O'Leary, M. E., and Chahine, M. (2011). Y1767C, a novel SCN5A mutation, induces a persistent  $\text{Na}^+$  current and potentiates ranolazine inhibition of  $\text{Nav}1.5$  channels. *Am. J. Physiol. Heart Circ. Physiol.* 300, H288–H299. doi: 10.1152/ajpheart.00539.2010
- Iyer, V., Mazhari, R., and Winslow, R. L. (2004). A computational model of the human left-ventricular epicardial myocyte. *Biophys. J.* 87, 1507–1525. doi: 10.1529/biophysj.104.043299
- Jurman, M. E., Boland, L. M., Liu, Y., and Yellen, G. (1994). Visual identification of individual transfected cells for electrophysiology using antibody-coated beads. *Biotechniques* 17, 876–881.
- Li, G. R., Feng, J., Yue, L., and Carrier, M. (1998). Transmural heterogeneity of action potentials and  $\text{Ito}1$  in myocytes isolated from the human

- right ventricle. *Am. J. Physiol.* 275, H369–H377.
- Li, G. R., Yang, B., Feng, J., Bosch, R. F., Carrier, M., and Nattel, S. (1999). Transmembrane ICa contributes to rate-dependent changes of action potentials in human ventricular myocytes. *Am. J. Physiol.* 276, H98–H106.
- Margolskee, R. F., McHendry-Rinde, B., and Horn, R. (1993). Panning transfected cells for electrophysiological studies. *Biotechniques* 15, 906–911.
- Moreau, A., Keller, D. I., Huang, H., Fressart, V., Schmiel, C., Timour, Q., et al. (2012). Mexiletine differentially restores the trafficking defects caused by two brugada syndrome mutations. *Front. Pharmacol.* 3:62. doi: 10.3389/fphar.2012.00062
- Nagatomo, T., Fan, Z., Ye, B., Tonkovich, G. S., January, C. T., Kyle, J. W., et al. (1998). Temperature dependence of early and late currents in human cardiac wild-type and long Q-T DeltaKPC Na<sup>+</sup> channels. *Am. J. Physiol.* 275, H2016–H2024.
- Noble, D., and Noble, P. J. (2006). Late sodium current in the pathophysiology of cardiovascular disease: consequences of sodium-calcium overload. *Heart* 92(Suppl. 4), iv1–iv5. doi: 10.1136/hrt.2005.078782
- Pasek, M., Simurda, J., Orchard, C. H., and Christe, G. (2008). A model of the guinea-pig ventricular cardiac myocyte incorporating a transverse-axial tubular system. *Prog. Biophys. Mol. Biol.* 96, 258–280. doi: 10.1016/j.pbiomolbio.2007.07.022
- Pieske, B., and Houser, S. R. (2003). [Na<sup>+</sup>]<sub>i</sub> handling in the failing human heart. *Cardiovasc. Res.* 57, 874–886. doi: 10.1016/S0008-6363(02)00841-6
- Priebe, L., and Beuckelmann, D. J. (1998). Simulation study of cellular electric properties in heart failure. *Circ. Res.* 82, 1206–1223. doi: 10.1161/01.RES.82.11.1206
- Rush, A. M., Dib-Hajj, S. D., Liu, S., Cummins, T. R., Black, J. A., and Waxman, S. G. (2006). A single sodium channel mutation produces hyper- or hypoexcitability in different types of neurons. *Proc. Natl. Acad. Sci. U.S.A.* 103, 8245–8250. doi: 10.1073/pnas.0602813103
- Schwartz, P. J., Crotti, L., and Insolia, R. (2012). Long-QT syndrome: from genetics to management. *Circ. Arrhythm. Electrophysiol.* 5, 868–877. doi: 10.1161/CIRCEP.111.962019
- Schwartz, P. J., Priori, S. G., Spazzolini, C., Moss, A. J., Vincent, G. M., Napolitano, C., et al. (2001). Genotype-phenotype correlation in the long-QT syndrome: gene-specific triggers for life-threatening arrhythmias. *Circulation* 103, 89–95. doi: 10.1161/01.CIR.103.1.89
- Soliman, D., Wang, L., Hamming, K. S., Yang, W., Fatehi, M., Carter, C. C., et al. (2012). Late sodium current inhibition alone with ranolazine is sufficient to reduce ischemia- and cardiac glycoside-induced calcium overload and contractile dysfunction mediated by reverse-mode sodium/calcium exchange. *J. Pharmacol. Exp. Ther.* 343, 325–332. doi: 10.1124/jpet.112.196949
- Tan, H. L., Bardai, A., Shimizu, W., Moss, A. J., Schulze-Bahr, E., Noda, T., et al. (2006). Genotype-specific onset of arrhythmias in congenital long-QT syndrome: possible therapy implications. *Circulation* 114, 2096–2103. doi: 10.1161/CIRCULATIONAHA.106.642694
- Tang, Q., Ma, J., Zhang, P., Wan, W., Kong, L., and Wu, L. (2012). Persistent sodium current and Na<sup>(+)</sup>/H<sup>(+)</sup> exchange contributes to the augmentation of the reverse Na<sup>(+)</sup>/Ca<sup>(2+)</sup> exchange during hypoxia or acute ischemia in ventricular myocytes. *Pflugers Arch.* 463, 513–522. doi: 10.1007/s00424-011-1070-y
- Ten Tusscher, K. H., Bernus, O., Hren, R., and Panfilov, A. V. (2006). Comparison of electrophysiological models for human ventricular cells and tissues. *Prog. Biophys. Mol. Biol.* 90, 326–345. doi: 10.1016/j.pbiomolbio.2005.05.015
- Ten Tusscher, K. H., Noble, D., Noble, P. J., and Panfilov, A. V. (2004). A model for human ventricular tissue. *Am. J. Physiol. Heart Circ. Physiol.* 286, H1573–H1589. doi: 10.1152/ajpheart.00794.2003
- Undrovinas, A. I., Belardinelli, L., Undrovinas, N. A., and Sabbah, H. N. (2006). Ranolazine improves abnormal repolarization and contraction in left ventricular myocytes of dogs with heart failure by inhibiting late sodium current. *J. Cardiovasc. Electrophysiol.* 17(Suppl. 1), S169–S177. doi: 10.1111/j.1540-8167.2006.00401.x
- Vahedi, K., Depienne, C., Le Fort, D., Riant, F., Chaine, P., Trouillard, O., et al. (2009). Elicited repetitive daily blindness: a new phenotype associated with hemiplegic migraine and SCN1A mutations. *Neurology* 72, 1178–1183. doi: 10.1212/01.wnl.0000345393.53132.8c
- Viswanathan, P. C., and Rudy, Y. (1999). Pause induced early afterdepolarizations in the long QT syndrome: a simulation study. *Cardiovasc. Res.* 42, 530–542. doi: 10.1016/S0008-6363(99)00035-8
- Wong, J. A., Gula, L. J., Klein, G. J., Yee, R., Skanes, A. C., and Krahn, A. D. (2010). Utility of treadmill testing in identification and genotype prediction in long-QT syndrome. *Circ. Arrhythm. Electrophysiol.* 3, 120–125. doi: 10.1161/CIRCEP.109.907865

**Conflict of Interest Statement:** The authors declare that the research was conducted in the absence of any commercial or financial relationships that could be construed as a potential conflict of interest.

Received: 27 June 2013; accepted: 11 September 2013; published online: 01 October 2013.

Citation: Moreau A, Krahn AD, Gosselin-Badaroudine P, Klein GJ, Christé G, Vincent Y, Boutjdir M and Chahine M (2013) Sodium overload due to a persistent current that attenuates the arrhythmogenic potential of a novel LQT3 mutation. *Front. Pharmacol.* 4:126. doi: 10.3389/fphar.2013.00126

This article was submitted to *Pharmacology of Ion Channels and Channelopathies*, a section of the journal *Frontiers in Pharmacology*. Copyright © 2013 Moreau, Krahn, Gosselin-Badaroudine, Klein, Christé, Vincent, Boutjdir and Chahine. This is an open-access article distributed under the terms of the Creative Commons Attribution License (CC BY). The use, distribution or reproduction in other forums is permitted, provided the original author(s) or licensor are credited and that the original publication in this journal is cited, in accordance with accepted academic practice. No use, distribution or reproduction is permitted which does not comply with these terms.

## APPENDIX

Equations used in the TNNP model:

WT is a variable taking three possible values: WT = 1 for a pure WT cell, WT = 0.5 for the heterozygous condition and WT = 0 when all channels are mutated.

$$g_{NaWT} = WT \cdot 14.838$$

$$g_{NaQ1476R} = (1 - WT) \cdot 14.838 \cdot (1 - 0.02)$$

$$i_{NafastWT} = g_{NaWT} \cdot m_{WT}^3 \cdot h_{WT} \cdot (V - E_{Na})$$

$$m_{infWT} = \frac{1}{1 + e^{\frac{V+53.6}{-7.4}}}$$

$$i_{NafastQ1476R} = g_{NaQ1476R} \cdot m_{Q1476R}^3 \cdot h_{Q1476R} \cdot (V - E_{Na})$$

$$m_{infQ1476R} = \frac{1}{1 + e^{\frac{V+51.3}{-8.2}}}$$

$$\tau_m = \frac{0.5 \cdot \left( \frac{1}{101.6 \cdot e^{V \cdot 0.1135} + 0.022} + 68 \cdot e^{-0.0717 \cdot V} + 0.0001 \right)}{4.83}$$

$$h_{infWT} = \frac{1}{1 + e^{\frac{V+86.5}{4.4}}}$$

$$h_{infQ1476R} = \frac{1}{1 + e^{\frac{V+80.6}{4.3}}}$$

$$\tau_h = \frac{0.5 \cdot \left( \frac{1}{1.1381 \cdot 10^{-6} \cdot e^{-0.1017 \cdot V} + 6.537 \cdot e^{0.08016 \cdot V} + 0.0005} \right)}{4.83}$$

$$g_{NapsWT} = \frac{WT \cdot 14.838 \cdot 0.0019}{fm}$$

$$fm = 3$$

$$g_{NapsQ1476R} = \frac{(1 - WT) \cdot 14.838 \cdot (1 - 0.02) \cdot 0.0033}{fm}$$

$$i_{NapsWT} = g_{NapsWT} \cdot m_{infWT}^3 \cdot (V - E_{Na})$$

$$i_{NapsQ1476R} = g_{NapsQ1476R} \cdot m_{infQ1476R}^3 \cdot (V - E_{Na})$$

$$i_{Na} = i_{NafastWT} + i_{NafastQ1476R} + i_{NapsWT} + i_{NapsQ1476R}$$